Direct synthesis of nanocrystalline oxide powders by wet-chemical techniques

Vladimir V. Srdić[1,*], Ružica Djenadić[1,#], Marija Milanović[1], Nikolina Pavlović[1], Ivan Stijepović[1], Ljubica M. Nikolić[1], Evagelia Moshopoulous[2], Konstantinos Giannakopoulos[2], Jan Dusza[3], Karel Maca[4]

[1]*Department of Materials Engineering, Faculty of Technology, University of Novi Sad, Novi Sad, Serbia*
[2]*Institute of Materials Science, National Centre for Scientific Research "Demokritos", Athens, Greece*
[3]*Institute of Materials Research, Slovak Academy of Sciences, Kosice, Slovakia*
[4]*Department of Ceramics and Polymers, Brno University of Technology, Brno, Czech Republic*

Received 16 June 2010; received in revised form 25 September 2010; accepted 29 September 2010

Abstract

In a recent period there is a great need for increasing the knowledge of tailoring the innovative procedures for the synthesis of electroceramic nanopowders and materials with improved quality for specific application. In order to produce electroceramics with desirable microstructure and properties, synthesis of stoichiometric, ultra-fine and agglomerate free powders with narrow size distributions is one of the most important steps. Within this scope, in the present paper we summarize our recent results on direct synthesis of some important perovskites and ferrites nanopowders by wet-chemical techniques.

Keywords*: direct synthesis, nanopowders, electroceramics, perovskites, ferrites*

I. Introduction

Considerable research effort directed to synthesis and characterization of electroceramic materials has been driven in recent years by their potential applications in the manufacture of a variety of microelectronic devices (transducers and actuators, infrared sensors, electro-optic switches, nonvolatile computer memories etc.) [1–4]. It is well known that most properties of electroceramic materials change considerably when the crystalline size is decreased to the submicrometer regime and the composition is modified by doping. Thus, synthesis of stoichiometric, high-purity, ultra-fine and agglomerate free powders with narrow size distributions is the first and perhaps the most important step in producing electroceramics with desirable microstructure and properties. Several wet-chemical methods are available for synthesis of nanosize powder, such as sol-gel synthesis, hydrothermal reactions, coprecipitation, molten salt preparation and emulsion technique. These processes are based on complex solution chemistry, require little capital investment and enable the production of relatively large quantities of high purity powders of very fine particle size. However, only techniques for the direct synthesis of crystalline nanoparticles are promising, as they enable elimination of calcination step usually responsible for considerably particle coarsening and the hard agglomerate formation. Several papers based on low-temperature synthesis of crystalline perovskite [5–8] or ferrite [9–11] particles were published recently. In most of the works homogeneous distribution of cations on atomic scale was already maintained in solution, which enables reaction at relatively low temperature and formation of homogeneous and stoichiometric nanocrystalline particles. In the present paper we summarize our recent work on direct synthesis of some important perovskite and ferrite powders by wet-chemical techniques.

II. Perovskite nanopowders

Nanocrystalline titanate ($SrTiO_3$, $PbTiO_3$, $La_{2/3}TiO_3$, $Bi_4Ti_3O_{12}$) powders were synthesized using a two-step process: first by controlled hydrolysis of titanium-butoxide ($Ti(OC_4H_9)_4$, Fluka) with distilled water, and then by

* Corresponding author: +381 21 485 3665
fax: +381 21 450 413, e-mail: *srdicvv@uns.ac.rs*
 # Now at Nanoparticle Preocess Technology, Department of Engineering Sciences, University Diusburg - Essen, Germany

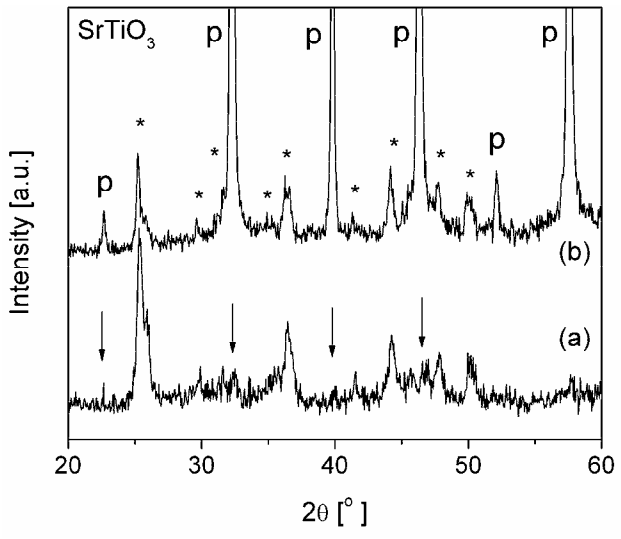

Figure 1. XRD patterns of $SrTiO_3$ nanopowders synthesized at: a) 20°C and b) 80°C (p – cubic $SrTiO_3$, * – $SrCO_3$)

further reaction of the formed hydrated titania gel particles with corresponding cations under different reaction conditions in a strong alkaline solution (pH > 13) [12,13]. The synthesis was conducted first by hydrolysis of $Ti(OC_4H_9)_4$ dissolved in anhydrous ethanol with distilled water. The obtained white titania sol was added to NaOH aqueous solution under vigorous stirring to precipitate the titanium hydroxide gel. Then an aqueous solution containing Sr^{2+} (from strontium nitrate ($Sr(NO_3)_2$, Fluka), Pb^{2+} (from lead acetate ($Pb(CH_3COO)_2 \times 3H_2O$, Aldrich, USA), Bi^{3+} (form bismuth(III)-nitrate pentahydrate ($Bi(NO_3)_3 \times 5H_2O$, Fluka) or La^{3+} (from lanthanum nitrate ($La(NO_3)_3 \times 6H_2O$, Riedel-de-Haen) was slowly added to the prepared slurry, and the reaction between titanium hydroxide particles and corresponding ions was carried out at different temperatures (over a period of 60 min): i) up to 80°C at ambient pressure or ii) up to 165°C under the hydrothermal conditions. The precipitated powders were collected with a centrifuge and washed several times with distilled water to expel sodium ions and then with absolute ethanol to decrease powder agglomeration by removing free water and replace the particle surface hydroxyl with ethoxy groups. The washed powders were dried at 120°C for 1 day in air.

2.1 Strontium titanate powders

Direct synthesis of crystalline strontium titanate particles is based on the reaction between the hydrolyzed titanium alkoxide and Sr^{2+} ions in a highly alkaline solution. In the first step, the highly porous titanium hydrous gel, exhibiting a fine, porous network structure and a very high surface area, 260 m^2/g, is formed [12]. In the second step, the amorphous titanium hydrous gel is infiltrated by aqueous $Sr(NO_3)_2$ solution, and soluble Sr^{2+} ions are first attached to the surface of the porous titanium hydroxide gel and then incorporated into the gel structure, forming perovskite $SrTiO_3$ phase.

The $SrTiO_3$ powder synthesized at 20°C has a very high surface area (192 m^2/g) and contains only traces of the perovskite phase, whereas sharp peaks of the crystalline cubic perovskite phase are present in the $SrTiO_3$ powder synthesized at 80°C (Fig. 1). Both samples contain $SrCO_3$, as an impurity phase, which is unavoidable unless great care is taken to ensure that the precursors and the reaction environment are CO_2-free [5,14]. However, the intensity of the $SrCO_3$ peaks in the XRD pattern of the sample synthesized at 20°C is considerably higher than for the sample synthesized at 80°C. This was explained [12] by the fact that at 20°C incorporation of Sr^{2+} ions into the porous gel structure is very slow, and they are mostly consumed in the much faster reaction with CO_2. Thus, the powder synthesized at 20°C consists of an amorphous titania phase, small portion of $SrTiO_3$ and considerable amount of extremely fine $SrCO_3$ crystallites. On the other side, at higher synthesis temperature of 80°C the favourable processes are incorporation of Sr^{2+} ions into the titanium hydrous gel structure, interaction with it and formation of the crystalline $SrTiO_3$ phase. As the reaction between Sr^{2+} and the titania gel is relatively fast at 80°C, only a part of Sr^{2+} ions is spent in the reaction with CO_2, and the nanopowder with dominant perovskite phase and a

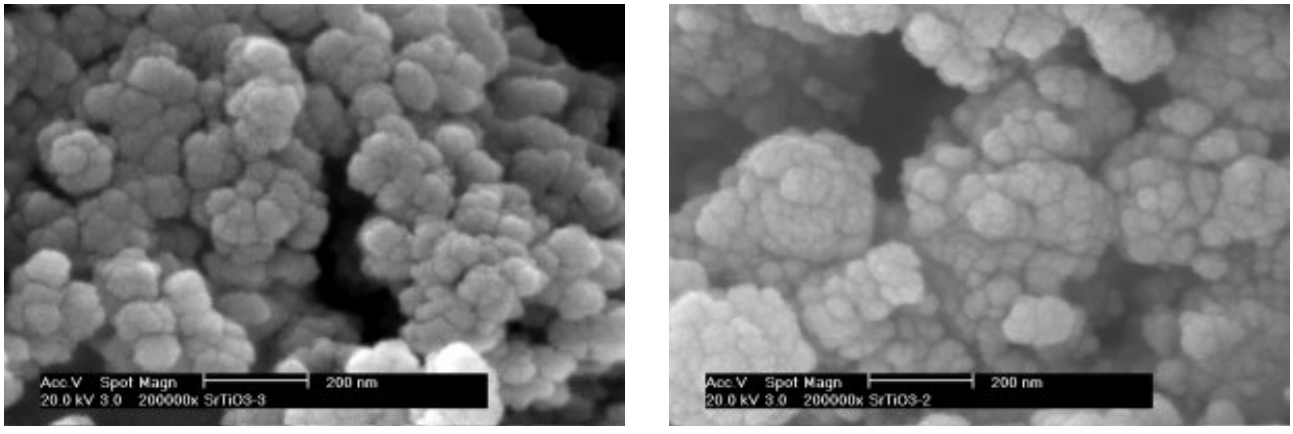

a) **b)**

Figure 2. HRSEM micrographs of $SrTiO_3$ nanopowders synthesized at: a) 20°C and b) 80°C

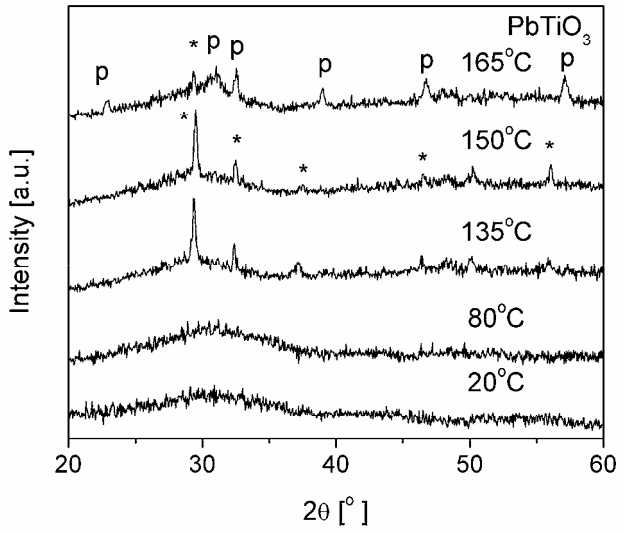

Figure 3. XRD patterns of $PbTiO_3$ powders synthesized at different temperatures: 20, 80, 135, 150 and 165°C for 60 minutes (p – tetragonal $PbTiO_3$, * – PbO-TiO_2 solid solution)

small amount of $SrCO_3$ is formed. The powders synthesized at 20 and 80°C are agglomerated (Fig. 2), with the primary particle size in nanometer range 32 nm and 37 nm, respectively.

2.2 Lead titanate powders

Direct synthesis of crystalline lead titanate particles is based on the reaction between the hydrolyzed titanium alkoxide and Pb^{2+} ions (from an aqueous $Pb(CH_3COO)_2$ solution) in a highly alkaline solution [12]. It is believed that the relatively soluble Pb^{2+} ions easy cover the entire surface of the porous titanium hydroxide gel, than slowly incorporate into the gel structure and finally form Ti-O-Pb bonds. If the reaction is carried out at low temperature (20 and even 80°C) there is not enough energy for the nucleation of $PbTiO_3$ phase, and the as-synthesized powders are completely XRD amorphous (Fig. 3). However, the amorphous structure can be directly transformed into the perovskite $PbTiO_3$ phase after calcination at around 500°C [12]. Both powders (synthesized at 20 and 80°C) consist of very fine amorphous particles with the average size of about 20 nm (Fig. 4a) and have very high surface areas (149 and 147 m^2/g, respectively).

Crystalline phase was directly synthesized in the reaction of Pb^{2+} ions with the titanium hydrous gel at high temperature, i.e. under the hydrothermal conditions (Fig. 3). Thus, an intermediate crystalline phase was obtained at 135 and 150°C, whereas perovskite $PbTiO_3$

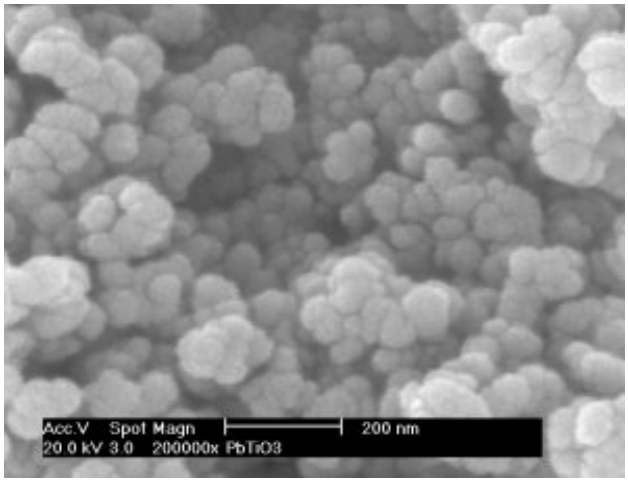

a)

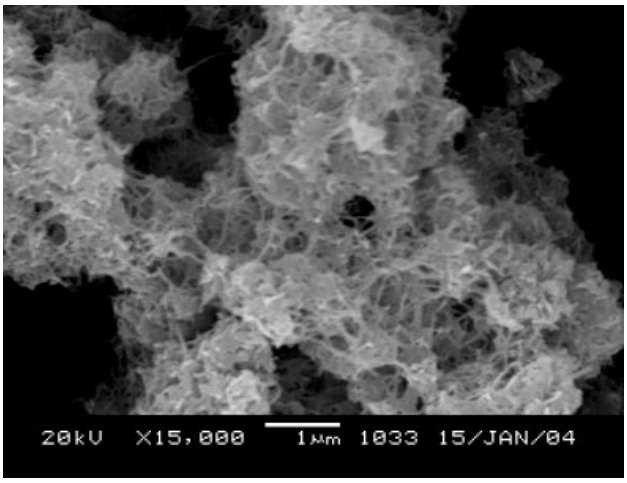

b)

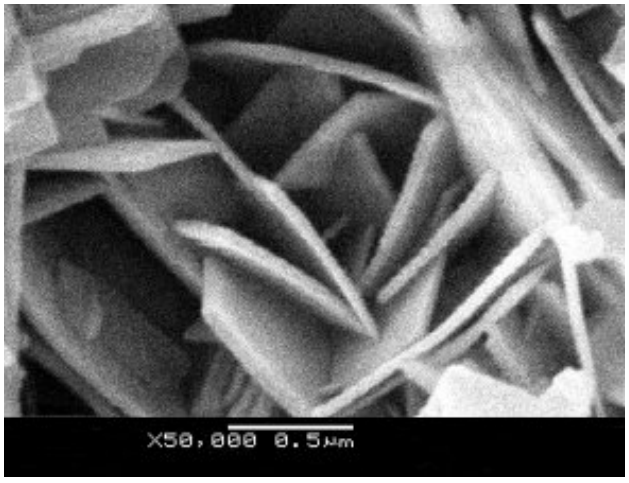

c)

Figure 4. SEM micrographs of $PbTiO_3$ powders synthesized at: a) 20°C, b) 135°C and c) 150°C

phase was formed at 165°C. Pure perovskite $PbTiO_3$ phase can be also formed in the hydrothermal reaction conducted at 150°C, but for somewhat longer period of 180 minutes (Fig. 5). The obtained results confirm that only hydrothermal conditions provide enough energy, necessary not only for rearrangement of the titania gel structure by incorporating of Pb^{2+} ions initially adsorbed on its surfaces, but also for nucleation of crystalline lead titanate phases.

Depending on processing conditions as-synthesized powders can have different morphology, starting from spherical nanoparticles (Fig. 4a), to platelet-like structure (Fig. 4c) or even a complex structures involving titanate particles covered with one-dimensional nanostructured elements (Fig. 4b).

2.3 Lanthanum titanate powders

$La_{2/3}TiO_3$ nanopowders were prepared in the reaction between the hydrolyzed titanium alkoxide and La^{3+} ions in a highly alkaline solution. XRD presented in Fig. 6 shown that the powder synthesized at 20°C (and even at 80°C) consists of almost pure $La(OH)_3$ phase. Formation of $La(OH)_3$ phase is favourable even under the hydrothermal conditions, and at 110°C only a small amount of perovskite phase is obtained (indicated by arrows in Fig. 6). This means that, like the $SrTiO_3$ system, incorporation of La^{3+} ions in the titanium hydrous gel structure is impeded by the formation of an impurity phase. On the other side, different behaviour between strontium and lead in the process of titanate formation may be found in the nature of these elements, because Sr, an alkaline earth metal, reacts easily with CO_2 and Sr-O bond does not possess a partial covalent character like Pb-O bond.

2.4 Bismuth titanate powders

Bismuth titanate powders ($Bi_{4-x}A_xTi_3O_{12}$, where A = La or Ce and $x \leq 1$) were synthesized by aforementioned sol-gel process modified in a way that bismuth, cerium or lanthanum precursors were first dissolved in nitric acid and then mixed with hydrated titinia gel particles. All as-synthesized powders consist of very fine particles with the size in the nanometer range and with relatively high values of specific surface areas (~160 m^2/g). Since X-ray diffraction data revealed that as-synthesized powders are amorphous, thermal analyses were performed in order to determine the crystallization temperature required to obtain bismuth titanate phase, Fig. 7. The first exothermic peak on the DTA curve at around 290°C can be attributed to decomposition of residual organics and nitrates. The second exothermic effect, observed around 520°C for the pure bismuth titanate powder (sample $Bi_4Ti_3O_{12}$), can be attributed to crystallization of bismuth titanate [15]. After calcination at 600°C /1h a rapid drop in the specific surface area in the $Bi_4Ti_3O_{12}$ powders was observed (from 160 to 15.5 m^2/g) and crystalline nanoparticles were obtai-

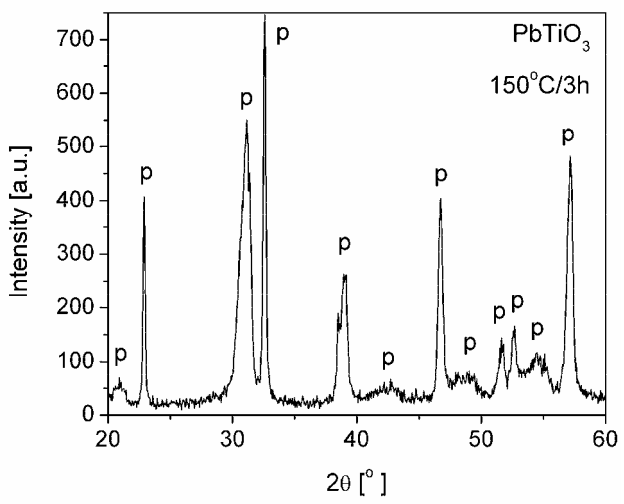

Figure 5. XRD patterns of $PbTiO_3$ powders synthesized at 150°C for 180 minutes (p – tetragonal $PbTiO_3$)

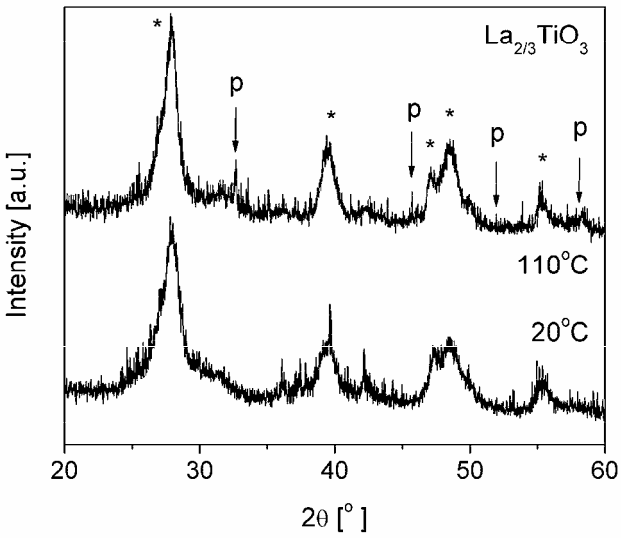

Figure 6. XRD patterns of $La_{2/3}TiO_3$ powders synthesized at 20°C and 110°C (p – $La_{2/3}TiO_3$, * – $La(OH)_3$)

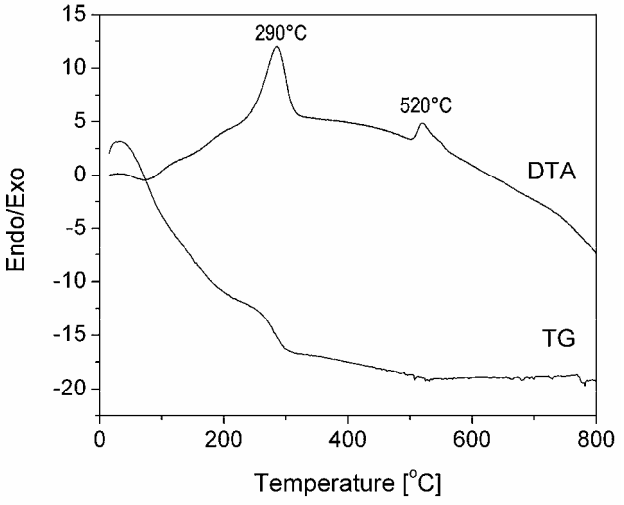

Figure 7. DTA curves of as-synthesized bismuth titanate nanopowders

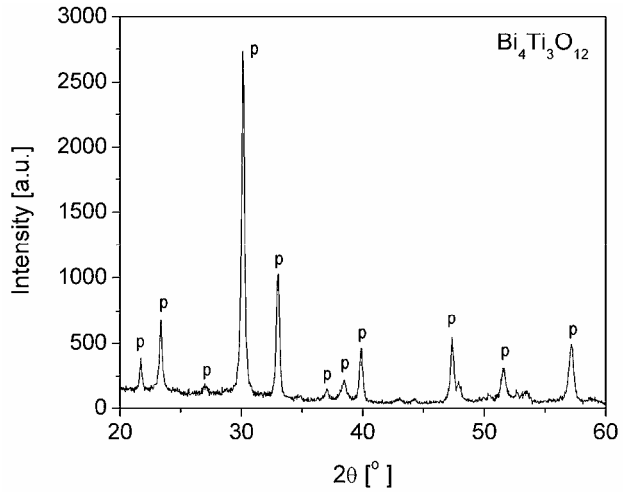

Figure 8. XRD patterns of wet-chemically synthesized $Bi_4Ti_3O_{12}$ nanopowders (p – $Bi_4Ti_3O_{12}$)

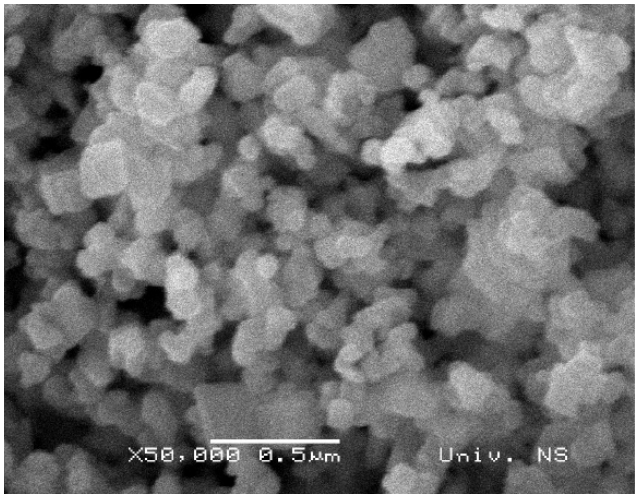

Figure 9. SEM micrographs of $Bi_4Ti_3O_{12}$ nanopowder

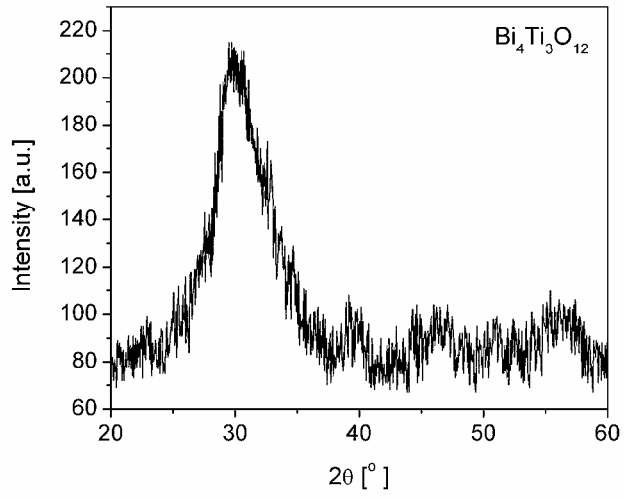

Figure 10. XRD patterns of hydrothermally synthesized $Bi_4Ti_3O_{12}$ powders

ned. It is interesting to note that XRD peaks at 2θ angles of ~32°, ~40° and ~58° are unseparated, indicating that the calcined unmodified powder has tetragonal structure, Fig. 8. Since tetragonal $Bi_4Ti_3O_{12}$ is stable only above Curie temperature, the presence of tetragonal structure at room temperature could be due to kinetics [16] and/or size effect [17]. Micrographs of the calcined powder (Fig. 9) confirm that powder consists of agglomerates of fine equiaxial-shaped particles, however, sinterability of the obtained particles are good and almost fully dense ceramics can be processed even after uneasily pressing and pressure-less sintering [13].

Crystalline phase was directly synthesized in the reaction of Bi^{3+} ions with the titanium hydrous gel at high temperature, i.e. under the hydrothermal conditions at 160°C (Fig. 10). Since the reaction time was short, the characteristics XRD peaks are very broad and not defined well. However, work of Xu *et al*. [18] showed that with prolonged hydrothermal reaction (for 30 or even 50 hours) fully crystallized bismuth-titanate particles can be formed. This additionally confirmed that even the more complex perovskite structure can be directly synthesised by wet-chemical techniques.

III. Ferrite nanopowders

Pure zinc ferrite ($ZnFe_2O_4$) and doped zinc ferrite ($Zn_{1-x}In_xFe_2O_4$ and $ZnY_xFe_{2-x}O_4$) nanoparticles were prepared by a low-temperature chemical co-precipitation method using aqueous solutions of nitrate precursors [19]. Stoichiometric amounts of $Fe(NO_3)_3{\times}9H_2O$ (Merck) and $Zn(NO_3)_2{\times}6H_2O$ (Merck) were dissolved in distilled water, mixed with appropriate amount of aqueous $InCl_3$ or YCl_3 solution and precipitated with a hydroxide solution (NH_4OH or NaOH). The co-precipitation reaction was carried out at different temperatures up to 95°C for 60 minutes under continuous stirring. The precipitates were separated from the slurry by centrifuging and washed a number of times with distilled water and then with absolute ethanol. The formed nanoparticles were dried at 120ºC for 1 day and finally dry milled in a mortar.

3.1 Zinc ferrite nanoparticles

The zinc-ferrite powders, synthesized at 20°C and 60°C with NH_4OH, are amorphous (Fig. 11) and crystallize after calcination at temperature between 550 and 600°C. However, both powders calcined at 600°C consist of mixture of the spinel $ZnFe_2O_4$ phase and the pure oxide phases. If the precipitation was carried out in presence of NaOH at 20°C the obtained powder is also amorphous (Fig. 11) confirming that the direct synthesis of crystalline $ZnFe_2O_4$ particles is not possible in the presence of NH_4OH or at room temperature. On the other hand, in presence of NaOH, crystalline powders, having the average crystallite size of about 3–4 nm, can be directly synthesized at 80°C (Fig. 11). Corresponding HRTEM im-

age (Fig. 12) implies that as-synthesized particles are uniform in size, well crystallized and agglomerated. With the increase of synthesis temperature to 95°C the single cubic spinel type is formed too, but the corresponding peaks are more sharp and narrow.

The lattice parameter of the as-prepared $ZnFe_2O_4$ nanoparticles (in presence of NaOH and at 80°C) is found to be a larger than the bulk zinc ferrite value [20], suggesting that they have a different crystal structure in terms of the distribution of the constituent cations over two lattice sites of the spinel structure compared to the bulk material [21]. These structural features will have a major impact on the magnetic properties of the studied system. And indeed, magnetic behaviour of the as-prepared $ZnFe_2O_4$, Fig. 13, has shown that in these nanoparticles, redistribution of cations occurred. Raman and Mössbauer measurements additionally confirmed the inversion of cations.

As-synthesized zinc ferrite nanoparticles show the characteristic hysteresis at 5 K with a high value of magnetization (M_s = 63.2 emu/g) which is a clear sign of ferrimagnetic ordering that originates from the difference in the magnetic moments of the ions at the octahedral and tetrahedral lattice sites, and thus directly reflects the distribution of the magnetic Fe^{3+} and non-magnetic Zn^{2+} ions between the two sublattices. On the other hand, the hysteresis completely vanishes at the temperature of 300 K (Fig. 13), while the S shape of the curve imply on the presence of single domain nanoparticles in superparamagnetic state. The obtained values of magnetization are much higher that the magnetization of bulk zinc ferrite [22,23], which together with the structural characteristics and high specific surface area (around 220 m^2/g), implies that nanoscaling in this system modifies the magnetic properties enabling the design of the magnetic ceramics with significantly improved properties compared to the bulk-counterparts.

3.2 Doped zinc-ferrite nanoparticles

In addition, we have investigated the possibility of introducing different cations (In^{3+} and Y^{3+}) in the spinel structure using the same one-step coprecipitation route. The results of X-ray analyses confirmed the nanosized nature and spinel type structure of the investigated samples, Figs. 14 and 15, which shows that the direct synthesis at low temperature can be applied even to obtain a complex oxide system (e.g. $Zn_{1-x}In_xFe_2O_4$ and $ZnY_xFe_{2-x}O_4$). It was found that yttrium and indium have a quite different influence on the structural characteristics of zinc ferrites. Addition of yttrium causes an increase of crystallite size, while increase of indium content influence the broadening of the XRD peaks, leading to decrease of crystallite size, Fig. 15. The reason for this is likely to be found in the synthesis of ferrite nanoparticles, where the addition of Y^{3+} ions in the solution of Fe^{3+} and Zn^{2+} ions increases the reaction rate and stimulates the formation of

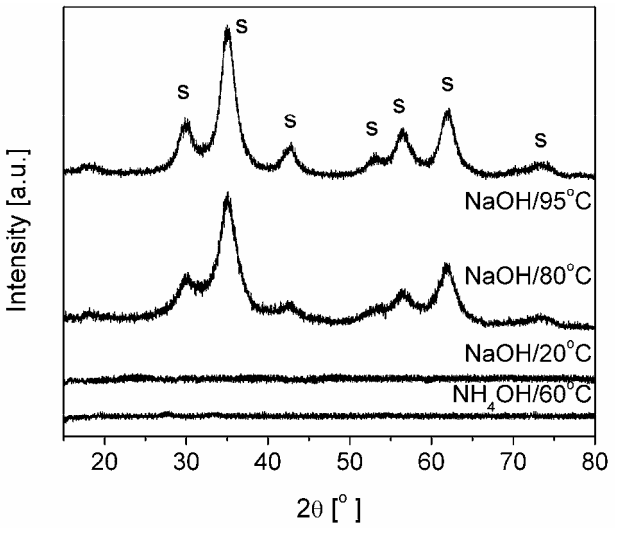

Figure 11. XRD patterns of $ZnFe_2O_4$ nanopowders obtained under different synthesis conditions (s – spinel ferrite)

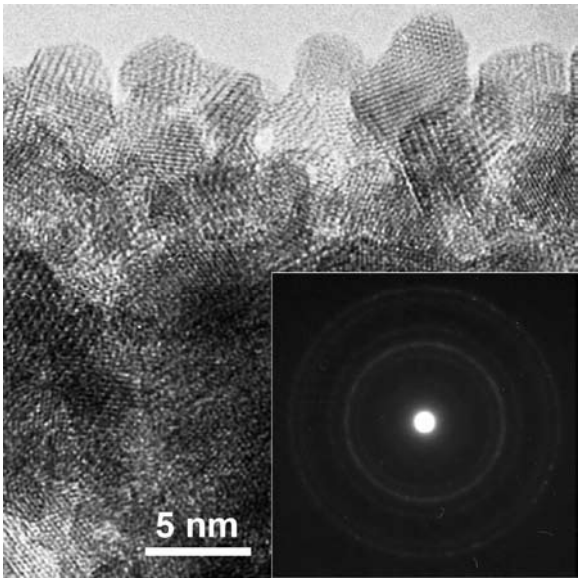

Figure 12. XRD pattern and HRTEM image of $ZnFe_2O_4$ nanoparticles synthesized in presence of NaOH and at 80°C

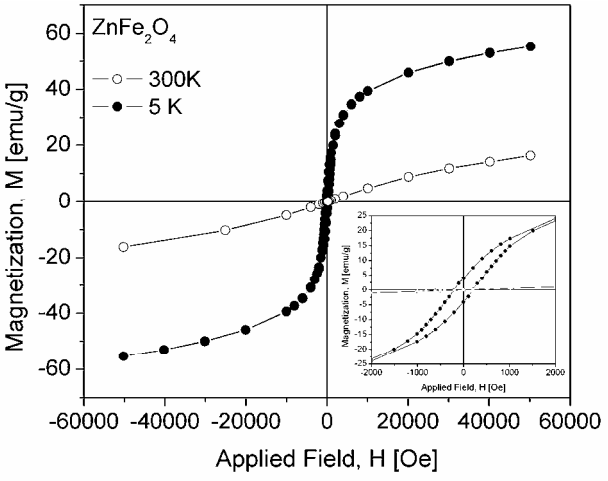

Figure 13. Magnetization of $ZnFe_2O_4$ nanoparticles as a function of the applied magnetic field at T = 5 K and T = 300 K

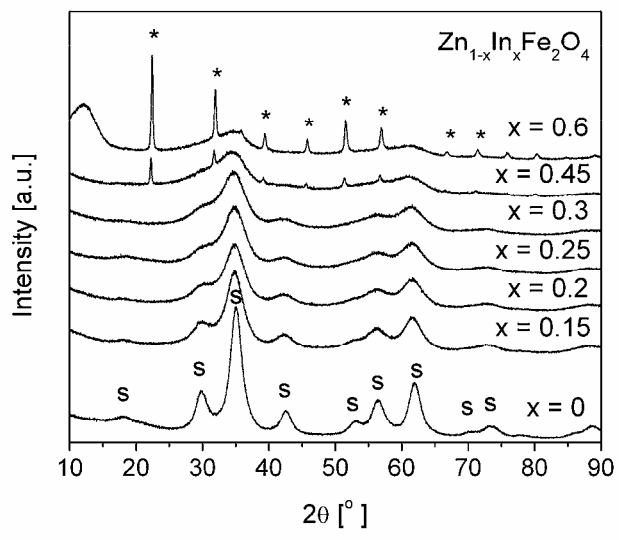

Figure 14. XRD patterns of $Zn_{1-x}In_xFe_2O_4$ nanoparticles (s – spinel ferrite, * - $In(OH)_3$)

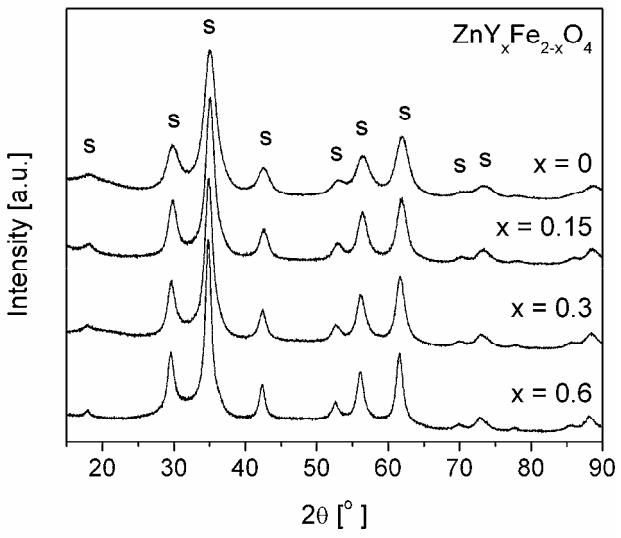

Figure 15. XRD patterns of $ZnY_xFe_{2-x}O_4$ nanoparticles (s – spinel ferrite)

highly crystalline zinc ferrite nanopowders. On the other hand, indium inhibits the phase transformation, resulting in a small crystallinity of zinc ferrite nanopowders doped with indium. However, what is interesting to note is that the addition of indium and yttrium has a positive effect on the particle size distribution, making it more uniform, as confirmed by TEM results shown in Fig. 16.

Raman and Mössbauer spectroscopy studies carried out on the indium- and yttrium-zinc ferrite nanoparticles implied on the possible cation distribution between the tetrahedral and octahedral sites and formation of the partially inversed spinel. The study of the magnetic properties showed that hysteresis loops do not saturate even in the presence of high magnetic fields, which confirmed the superparamagnetic and single domain nature of samples. These observations imply that, besides the particle size, composition (e.g. addition of yttrium and indium) causes significant structural rearrangements which in turn induce changes in magnetic behavior of the investigated nanoparticulate systems.

IV. Conclusions

Nanocrystalline ceramic powders have been prepared by using chemical synthesis routes under specific conditions. Our research showed that direct synthesis is promising concept in producing very high purity, high-quality and high surface area nanopowders without further calcination steps. Nanoceramic powders – single phase or two phase mixtures of $SrTiO_3$, $PbTiO_3$, $La_{2/3}TiO_3$, $Bi_4Ti_3O_{12}$, $ZnFe_2O_4$, $Zn_{1-x}In_xFe_2O_4$ and $ZnY_xFe_{2-x}O_4$ – with a wide range of powder properties for various targeted applications can be synthesized by varying: temperature, reaction time, pH, purity, dopant type and dopant concentration. The examples show the

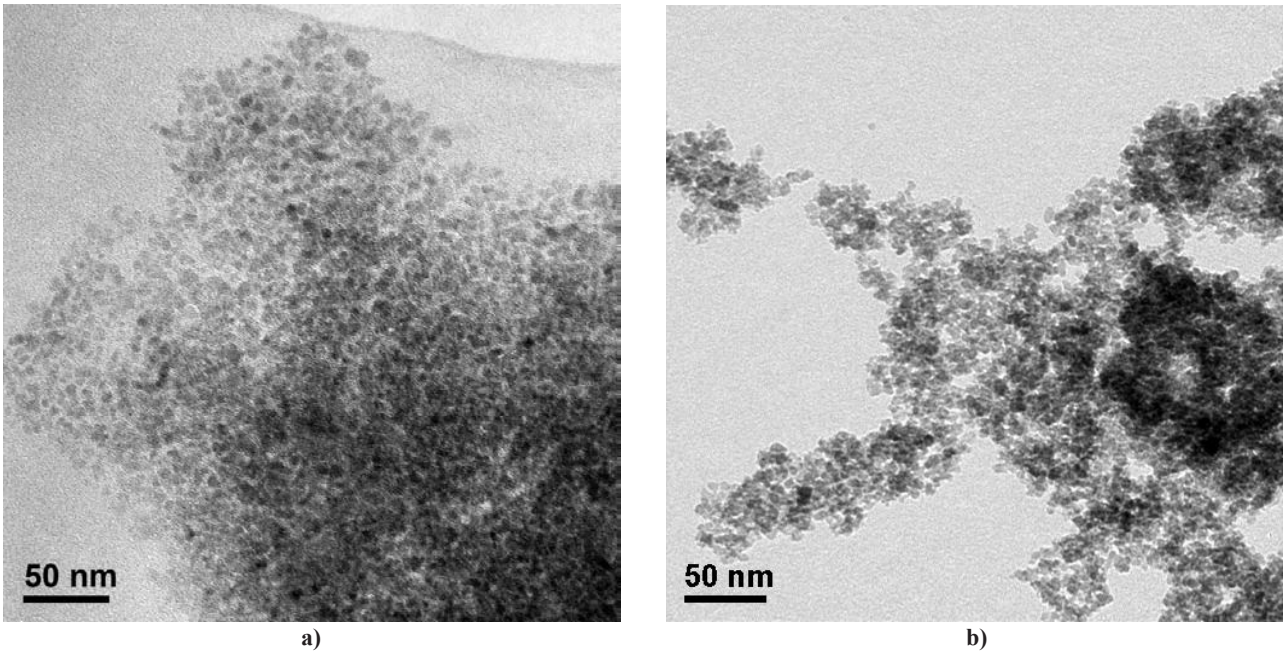

a) **b)**

Figure 16. TEM images of: a) $Zn_{0.85}In_{0.15}Fe_2O_4$ and b) $ZnY_{0.15}Fe_{1.85}O_4$ nanoparticles

usefulness of the chemical nanoparticle approach for advanced materials fabrication and the high potential of these materials for variety of applications.

Acknowledgements The cooperation under the COST 539 Action "Electroceramics from nanopowders produced by non-conventional methods" is highly acknowledged**.**

References

1. A. Goldman, *Handbook of Modern Ferromagnetic Materials*, Kluwer Academic Publishers, Boston-Dordrecht-London, 1999.
2. G.H. Haertling, "Ferroelectric ceramics: History and technology", *J. Am. Ceram. Soc.*, **82** [4] (1999) 797–818.
3. A.J. Moulson, J.M. Herbert, *Electroceramics: Materials, Properties and Applications*. John Wiley & Sons Ltd., New York, 2003.
4. J. Rodel, W. Jo, K.T.P. Seifert, E.-M. Anton, T. Granzow, "Perspective on the development of lead-free piezoceramics", *J. Am. Ceram. Soc.*, **92** [6] (2009) 1153–1177.
5. M.I. Diaz-Guemes, T.G. Carreno, C.J. Serna, J.M. Palacios, "Mechanism of formation of $MTiO_3$ (M=Sr or Ba) by the gel method", *J. Mater. Sci*., **24** (1989) 1011–1014.
6. S.B. Cho, J.S. Noh, M.M. Lencka, R.E. Riman, "Low temperature hydrothermal synthesis and formation mechanisms of lead titanate ($PbTiO_3$) particles using tetramethylammonium hydroxide: Thermodynamic modelling and experimental verification", *J. Euro. Ceram. Soc.*, **23** (2003) 2323–2335.
7. M. Viviani, J. Lemaitre, M.T. Buscaglia, P. Nanni, "Low-temperature aqueous synthesis (LTAS) of $BaTiO_3$: a ststistical design of experiment approach", *J. Eur. Ceram. Soc.*, **20** (2000) 315–320.
8. M. Viviani, M.T. Buscaglia, A. Testino, V. Buscaglia, P. Bowen, P. Nanni, "The influence of concentration on the formation of $BaTiO_3$ by direct reaction of $TiCl_4$ with $Ba(OH)_2$ in aqueeous solution", *J. Eur. Ceram. Soc.*, **23** (2003) 1383–1390.
9. M. Ueda, S. Shimada, M. Inagaki, "Low temperature synthesis of zinc ferrite using hydrazine monohydrate", *J. Eur. Ceram. Soc.*, **15** (1995) 265–269.
10. Y. Zhihao, Z. Lide, "Synthesis and structural characterization of capped $ZnFe_2O_4$ nanoparticles", *Mater. Res. Bull.*, **33** [11] (1998) 1587–1592.
11. S. Verma, S.D. Pradhan, R. Pasricha, S.R. Sainkar, P.A. Joy, "A novel low-temperature synthesis of nanosized NiZn ferrite", *J. Am. Ceram. Soc.*, **88** [9] (2005) 2597–2599.
12. V.V. Srdić, R.R. Djenadić, "Nanocrystalline titanate powders: Synthesis and mechanisms of perovskite particles formation", *J. Optoelectr. Advanced Mater.*, **7** [6] (2005) 3005–3011.
13. N. Pavlović, V.V. Srdić, "Synthesis and structural characterization of Ce doped bismuth titanate", *Mater. Res. Bull.*, **44** [4] (2009) 860–864.
14. I. MacLaren, C.B. Ponton, "A TEM and HREM study of particle formation during barium titanate synthesis in aqueous solution", *J. Eur. Ceram. Soc.*, **20** (2000) 1267–1275.
15. S.H. Ng, J. Xue, J. Wang, "Bismuth titanate from mechanical activation of chemically coprecipitated precursor", *J. Am. Ceram. Soc*., **85** (2002) 2660–2665.
16. Y. Kan, P. Wang, Y.Li, Y. Cheng, D. Yan, "Low-temperature sintering of $Bi_4Ti_3O_{12}$ derived from co-precipitation method", *Mater. Lett.*, **56** (2002) 910–913.
17. W. S. Cho, E. Hamada, "Synthesis of ultrafine $BaTiO_3$ particles from polymeric precursor: their structure and surface property", *J. Alloys Compd.*, **266** (1998) 118–124.
18. H. Xu, K.J. Bowman, E.B. Slamovich, "Hydrothermal synthesis of bismuth titanate powders", *J. Am. Ceram. Soc*., **86** [10] (2003) 1815–1817.
19. M. Maletin, E.G. Moshopoulou, A.G. Kontos, E. Devlin, A. Delimitis, V.T. Zaspalis, L. Nalbandian, V.V. Srdić, "Synthesis and structural characterization of In-doped $ZnFe_2O_4$ nanoparticles", *J. Eur. Ceram. Soc.*, **27** (2007) 4391–4394.
20. K.E. Sickafus, J.W. Wills, N.W. Grimes, "Structure of spinel", *J. Am. Ceram. Soc.*, **82** (1999) 3279–3292.
21. D. Makovec, M. Drofenik, "Non-stoichiometric zinc-ferrite spinel nanoparticles", *J. Nanoparti. Res.*, **10** (2008) 131–141.
22. M.R. Anantharaman, S. Jagatheesan, K.A. Malini, S. Sindhu, A. Narayanasamy, C.N. Chinnasamy, J.P. Jacobs, S. Reijne, K. Seshan, R.H.H. Smits, H.H. Brongersma, "On the magnetic properties of ultra-fine zinc ferrites", *J. Magn. Magn. Mater.*, **189** (1998) 83–88.
23. C.N. Chinnasamy, A. Narayanasamy, N. Ponpandian, K. Chattopadhyay, H. Guérault, J.-M. Greneche, "Magnetic properties of nanostructured ferrimagnetic zinc ferrite", *J. Phys.: Condes. Matter.*, **12** (2000) 7795–7805.